

# Shear performance of an innovative UHPFRC deck of composite bridge with coarse aggregate

Jianan Qi<sup>\*</sup>, Jingquan Wang<sup>a</sup> and Yu Feng<sup>b</sup>

Key Laboratory of Concrete and Prestressed Concrete Structures of the Ministry of Education, School of Civil Engineering, Southeast University, Nanjing, China

(Received December 13, 2018, Revised April 1, 2019, Accepted April 5, 2019)

**Abstract.** This paper presents an experimental study on the structural performance of an innovative ultra-high performance fiber reinforced concrete (UHPFRC) deck with coarse aggregate of composite bridge under shear force. Test parameters included curing method and shear span-to-height ratio. Test results indicated that more short fine cracks developed beside the existing cracks due to the randomly dispersed fibers, resulting in re-distributing and homogenizing of the concrete stress beside cracks and allowing for the occurrence of more cracks with small spacing compared to normal strength concrete beams. Curing methods, incorporating steam curing and natural curing, did not have obvious effect on the nominal bending cracking strength and the ultimate strength of the test specimens. Shear reinforcement need not be provided for UHPFRC decks with a fiber volume fraction of 2%. UHPFRC decks showed superior load resistance ability after the appearance of cracks and excellent post-cracking deformability. Lastly, the current shear provisions were evaluated by the test results.

**Keywords:** composite bridge; deck; ultra-high performance fiber reinforced concrete (UHPFRC); shear; steel fiber

## 1. Introduction

Steel-concrete composite bridges, which take advantage of the high tensile strength of steel and high compressive strength of concrete, have been widely applied in bridge engineering during the last decades (Suwaed and Karavasilis 2018, Qi *et al.* 2017b, Wang *et al.* 2019). However, a great deal of steel-concrete composite cable-stayed bridge suffered from the problem of concrete bridge deck cracking (Walter *et al.* 2007, Qi *et al.* 2018a). Traditionally, the structural and construction measurements, such as increasing the deck thickness, increasing the reinforcement ratio and applying the prestressing technology, are used to prevent the concrete bridge deck cracking. The engineering practice revealed that these methods could not solve the problem completely.

An alternative way to solve the concrete bridge deck cracking problem is to develop an innovative ultra-high performance fiber reinforced concrete (UHPFRC) deck with the aim to decrease the self-weight of the bridge main girder and to reduce the cracking risk of concrete bridge deck. UHPFRC is supposed to be an advanced cementitious composite that exhibit superior levels of technical performance compared to conventional strength concrete in terms of material strength, ductility, durability and energy dissipation (Qi *et al.* 2017a, Qi *et al.* 2018c, Pourbaba *et al.* 2019). The tensile strength and ultimate tensile strain of

UHPFRC could be as high as 8MPa and 1% (Tran *et al.* 2015, Mosaberpanah and Eren 2017, Pourbaba *et al.* 2018). Thus, the thickness of the concrete bridge deck could be significantly reduced, resulting in a great decrement in the dead load of a bridge. In addition, a great deal of the reinforcement could be eliminated and a significant reduction in crack widths could be achieved by using UHPFRC (Sallem *et al.* 2011).

Some pioneering studies have been conducted to study the structural behavior of such thin bridge deck. Toutlemonde *et al.* (2005) pointed out that the application of UHPFRC could significantly decrease the cross section dimension and the self-weight of a bridge, and they presented an example of preliminary design on a (90+130+90) m highway bridge. Sallem *et al.* (2011) developed a lightweight ultra-high performance concrete-high strength steel (UHPC-HSS) bridge deck system with solid riding surfaces to replace the open-grid steel decks for moveable bridges. They found that shear failure was the governing failure mode in most of the specimens but was not abrupt and catastrophic. The optimal dimension for proposed UHPC-HSS deck system was 102 mm in height and the longitudinal reinforcement diameter of 16 mm should be provided to meet the design requirements (Ghasemi *et al.* 2016, Sallem *et al.* 2014). Lachance *et al.* (2016) compared the structural behavior of different slabs, including a high performance concrete cast-in-place slab, two fiber reinforced concrete precast slabs, one hybrid design using high performance fiber reinforced concrete and UHPFRC and one using only UHPFRC. The test results indicated that the hybrid and UHPFRC slabs exhibited minor crack widths in service and fatigue conditions. Harris and Roberts-Wollmann (2005) evaluated the punching shear capacity of thin ultra-high performance concrete (UHPC)

\*Corresponding author, Assistant Professor  
E-mail: [qijianan723@126.com](mailto:qijianan723@126.com)

<sup>a</sup>Professor

<sup>b</sup>Ph.D. Student

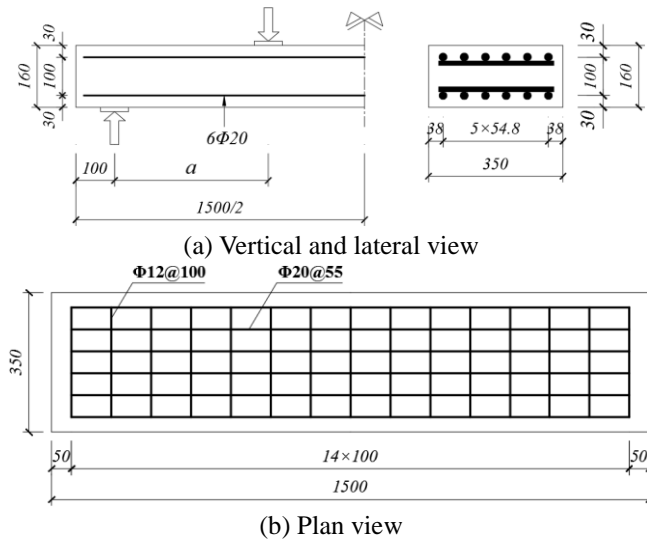


Fig. 1 Dimensions and cross section of test specimens

slabs via an experimental investigation on twelve 1143×1143 mm slabs. They pointed out that the minimum slab thickness was required to be 25.4 mm for a UHPC slab to prevent punching shear failure under 203×508 mm wheel load of 166 kN. Naaman and Chandransu (2004) developed a new high-performance fiber-reinforced cementitious composite deck system, in which only one layer of reinforcement is used. Whereafter, Naaman *et al.* (2007) carried out an experimental study on the effect of fibers on the punching shear behavior of high-performance fiber-reinforced cementitious composite slab panels and stated that the addition of fibers significantly improved the punching shear resistance due to the tensile strain hardening response and no spalling of concrete cover at large deformations.

In recent years, the addition of gravel coarse aggregates into UHPFRC has been gained increasingly attention as a method to further reduce the cost and to popularize the application of UHPFRC in civil engineering (Liu *et al.* 2016, Wang *et al.* 2012). Several advantages could be achieved by adding gravel coarse aggregates, such as increasing the stiffness, decreasing the amount of binder material and the total cost, lowering the risk of cracking, controlling shrinkage and so on (Liu *et al.* 2016, Ma *et al.* 2004). Nevertheless, some disadvantages may also arise due to the addition of gravel coarse aggregates. For example, the space for the dispersion of fibers is reduced, resulting in the reunion of fibers and decreasing the resistance on cracks (Akçaoğlu *et al.* 2004, Tasdemir *et al.* 1996). Therefore, a comprehensive understanding is needed in order to obtain a better understanding of the shear performance and the popularization of UHPFRC decks with coarse aggregate in engineering practice.

To the best of the authors' knowledge, however, no public report to date has specifically focused on the shear behavior of UHPFRC decks with coarse aggregate. Therefore, this study aims at investigating the shear performance of an innovative UHPFRC deck with coarse aggregate via an experimental programme on sixteen UHPFRC decks with the parameters of curing method and

Table 1 UHPC deck properties

Specimen ID	$a$ (mm)	$b$ (mm)	$h$ (mm)	$a/h$	Curing method
S2.5-A-1	400	350	160	2.5	A
S2.5-A-2	400	350	160	2.5	A
S2.5-C-1	400	350	160	2.5	C
S2.5-C-2	400	350	160	2.5	C
S2-A-1	320	350	160	2	A
S2-A-2	320	350	160	2	A
S2-C-1	320	350	160	2	C
S2-C-2	320	350	160	2	C
S1.5-A-1	240	350	160	1.5	A
S1.5-A-2	240	350	160	1.5	A
S1.5-C-1	240	350	160	1.5	C
S1.5-C-2	240	350	160	1.5	C
S1-A-1	160	350	160	1	A
S1-A-2	160	350	160	1	A
S1-C-1	160	350	160	1	C
S1-C-2	160	350	160	1	C

Note:  $b$ =width of the web;  $h$ =deck height;  $a/h$ =shear span-to-height ratio; A=steam curing; C=natural curing.

shear span-to-height ratio. The post-cracking behavior with regards to global behavior, post-cracking capacity and post-cracking deformability were explicitly discussed based on the test results. It was found that the proposed UHPFRC deck showed superior load resistance after the appearance of cracks and excellent post-cracking deformability. Lastly, the current shear provisions were evaluated using the experimental data.

## 2. Experimental program

### 2.1 Specimen dimensions and test parameters

A total of sixteen slabs, as shown in Fig. 1 and Table 1, were built and tested to failure to investigate the structural performance of an innovative UHPFRC deck of composite bridge under shear force. All the specimens were simply supported with the test parameters of curing method and shear span-to-height ratio. Two curing methods, including steam curing (A) and natural curing (C), were used in the test program. Four shear span-to-height ratios, namely 1, 1.5, 2 and 2.5, were designed. Specimen ID was designated using the test parameters. For example, "S2.5-A-1" refers to the first specimen in the series "S2.5-A" with a shear span-to-height ratio of 2.5 using steam curing method.

All sixteen specimens had the same geometric dimension, cross section and reinforcement arrangement. The length of the specimen was 1500 mm, while the pure span was 1300 mm. The height and the web width of the cross section were 160 mm and 350 mm, respectively. The specimen was reinforced with longitudinal reinforcement and transverse reinforcement. Six deformed steel bars with a diameter of 20 mm were embedded in the bottom, as well as the top, of the specimen, which led to a longitudinal reinforcement ratio of 4.14%. The diameter and spacing of the transverse reinforcement were 12 mm and 100 mm, respectively. It should be noted that all the specimens were



Fig. 2 Test setup

designed without shear reinforcement.

## 2.2 Test setup and loading instrumentation

As presented in Fig. 2, two equal concentrated loads was monotonically applied using hydraulic screw jacks with a maximum capacity of 1000 kN, and the loads, specimen deflections, and the concrete and the reinforcement strains were simultaneously recorded at each loading stage. Before testing, the specimen was loaded to approximate 40% cracking load to examine the service performance of the instruments and then unloaded. During testing, the load was applied at 10 kN/min until 80% cracking load. Then, the load was decreased to 3 kN/min in order to obtain an accurate cracking load. After cracking, the loading rate was changed to 20 kN/min until about 80% maximum capacity, and subsequently 5 kN/min until maximum capacity. Lastly, the loading rate was set to 10 kN/min during unloading process.

## 2.3 Mix proportions and specimen preparation

The mixture proportions used in this study are summarized in Table 2. The components P II 52.5 cement and silica fume were included as cementitious materials and were commercially available in China. The density and specific surface area were  $3.17 \text{ g/cm}^3$  and  $388 \text{ m}^2/\text{kg}$ , respectively. Undeformed medium-coarse sand with 5 mm maximum particle size and 2.6 fineness modulus was used in the research. Since the designed UHPFRC has a relative low water to binder ratio and in order to improve the viscosity and mechanical performance of UHPFRC, a high active admixture named SBT® -PCA was developed. Unlike classic UHPFRC without coarse aggregate, broken stone with the diameter ranged from 5 mm to 8 mm and the specific surface area of  $2800 \text{ kg/m}^3$  was included as coarse aggregate in order to increase the stiffness and decrease the shrinkage. High strength steel fibers with a volume fraction of 2% were dispersed randomly to improve the strength and ductility of UHPFRC. As shown in Fig. 3, high strength straight steel fibers, coated with a thin layer of copper, were utilized in this study. The length and diameter of the steel fiber were 13 mm and 0.2 mm, respectively.

Field mixing of the innovative UHPFRC was conducted by the shaft mixer which provided a total volume of  $0.3 \text{ m}^3$  once. Cementitious material and aggregate needed to be dry-mixed for one minute first followed by adding water and additives to stir for four minutes. The high strength steel fibers should be put in terminally and continued

Table 2 Composition of UHPC

Component	Weight ( $\text{kg/m}^3$ )
Cement	732
Broken Stone 5-8mm	397
Sand 0-5mm	737
Silica fume	85
High active admixture	299
Steel fiber	160
Water	165
Superplasticizer	22.7
Water-binder ratio (W/B)	0.16

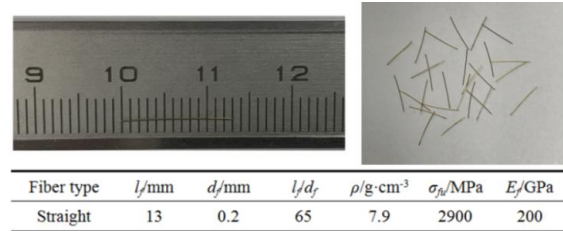


Fig. 3 Steel fiber

stirring for three minutes. Matrix of the UHPFRC could be poured out for the specimens forming after mixing evenly, and this operation should run parallel to the casting of samples for material properties test.

As aforementioned, two curing methods were used in this study. The curing requirements were on the basic of the Chinese Code (GB/T 50081-2002). For steam curing, the temperature was increased to  $90^\circ\text{C}$  with an increment of  $10^\circ\text{C}/\text{h}$  and then maintained a constant value of  $90\pm 2^\circ\text{C}$  for 48h. After that, the temperature was decreased to the specimen surface temperature with a rate of  $10^\circ\text{C}/\text{h}$  and the temperature difference between the specimen surface and environment should not be more than  $20^\circ\text{C}$ . The humidity was  $\geq 95\%$ . For natural curing, the specimens were covered with plastic sheet and sprinkled with water.

## 2.4 Materials characterization

The material property tests for UHPFRC were conducted according to the Chinese Code (GB/T 31387-2015) except for the fracture energy test. The fracture energy test was carried out based on the Chinese Code CECS13-2009 (2009). Table 3 summarizes the material properties of UHPFRC and Fig. 4 shows the material property test photographs. Three cubic specimens with a dimension of  $100 \text{ mm}\times 100 \text{ mm}\times 100 \text{ mm}$  were used to determine the compressive strength. Six prism specimens were utilized to characterize the modulus of elasticity and the Poisson's ratio. The flexural strengths at cracking state and ultimate state were obtained from three  $100 \text{ mm}\times 100 \text{ mm}\times 400 \text{ mm}$  prism specimens using four point bending test. The fracture energy was determined by four  $100 \text{ mm}\times 100 \text{ mm}\times 400 \text{ mm}$  notched prism specimens.

Table 4 presents the material properties of reinforcements. Two types of deformed steel bars with diameters of 20 mm and 16 mm were used as the longitudinal reinforcement and the transverse reinforcement



Fig. 4 Material properties test

Table 3 Material properties of UHPC

Mix type	$E_c$ (GPa)	$\nu$	$f_{cu}$ (MPa)	$f_{MOR}$ (MPa)	$f_{MOR}^\dagger$ (MPa)	$G_F$ (J/m <sup>2</sup> )
A	50.4	0.20	165.7	13.6	19.9	24.6
C	49.3	0.21	146.7	12.7	17.1	24.1

Note:  $E_c$ =elasticity modulus;  $\nu$ =poisson's ratio;  $f_{cu}$ =cubic compressive strength;  $f_{MOR}$ =flexural strength at cracking state;  $f_{MOR}^\dagger$ =flexural strength at ultimate state;  $G_F$ =fracture energy.

Table 4 Material properties of reinforcement

Steel type	$d_s$ (mm)	$A_s$ (mm <sup>2</sup> )	$f_y$ (MPa)	$f_u$ (MPa)	$E_s$ (GPa)
Longitudinal reinforcement	20	314.2	350.5	582.5	200
Transverse reinforcement	12	113.1	446.6	566.3	200

Note:  $d_s$ =diameter;  $A_s$ =area;  $f_y$ =yield strength;  $f_u$ =ultimate strength;  $E_s$ =elasticity modulus.

in this experimental investigation. The yield strengths were 350.5 MPa and 446.6 MPa for the longitudinal reinforcement and the transverse reinforcement. The ultimate strengths were 582.5 MPa and 566.3 MPa for the longitudinal reinforcement and the transverse reinforcement.

### 3. Experimental results

#### 3.1 Failure mode and crack pattern

Fig. 5 and Fig. 6 respectively show the typical failure mode and crack pattern of the test specimen S2-A-1 at failure. Flexural cracks occurred first in the tension side adjacent to the mid-span cross section of the specimen with a nominal bending cracking strength  $\sigma_{cr}$  around 10 MPa. As the applied load increased, the number of cracks, corresponding to flexural cracks and shear cracks, increased whereas the crack width increased slightly. It is interesting to note that the width of shear cracks was larger than that of flexural cracks at this state. However, the propagation of shear cracks stopped as the load continued to increase whereas flexural cracks propagated rapidly. Unlike normal strength concrete members, test specimens exhibited multiple main cracks distribution with approximate equal



Fig. 5 Typical failure mode of test specimen S2-A-1

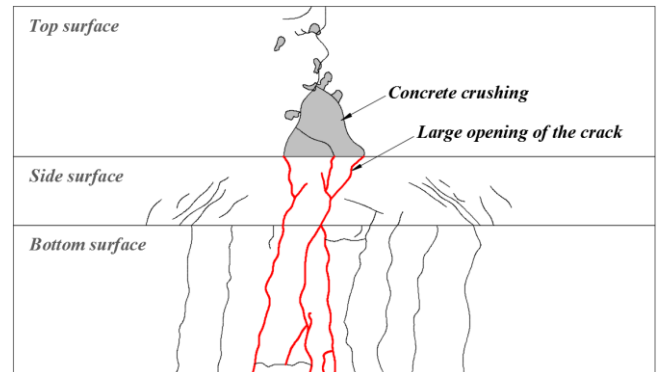


Fig. 6 Typical crack pattern of test specimen S2-A-1

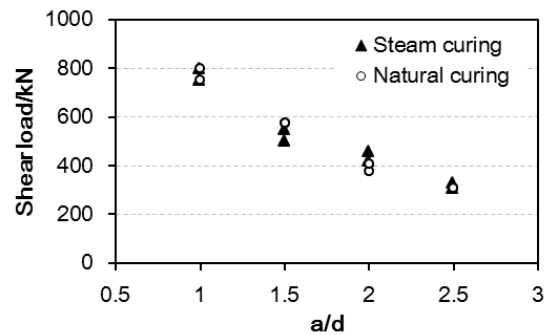


Fig. 7 Effect of test parameters on shear strength

spacing and large width within the pure bending region before failure. Finally, flexural failure occurred when the compression zone concrete reached to its strength and the tension side cracks opened too large.

#### 3.2 Shear strength and cracking strength

Table 5 summarizes the main test result at different states of the experiment. All the test specimens showed approximately the same nominal bending cracking strength at first cracking state because of the cracking strength being dominated by the material tensile strength of UHPFRC matrix. It is interesting to note that curing method did not have obvious effect on the nominal bending cracking strength at first cracking and the ultimate strength of the test specimens. This phenomenon indicates that cast-in-place method could be used for UHPFRC structures construction.

Fig. 7 presents the effect of test parameters on the shear strength of the test specimens. The shear strength decreased as the shear span-to-height ratio increased. However,

Table 5 Summary of test results

Specimen ID	First cracking			Crack width of 0.05 mm		Crack width of 0.10 mm		Crack width of 0.15 mm		Yielding state		Peak load		At failure	
	$V_{cr}$ (kN)	$\Delta_{cr}$ (mm)	$\sigma_{cr}$ (MPa)	$V_{0.05}$ (kN)	$\Delta_{0.05}$ (mm)	$V_{0.10}$ (kN)	$\Delta_{0.10}$ (mm)	$V_{0.15}$ (kN)	$\Delta_{0.15}$ (mm)	$V_y$ (kN)	$\Delta_y$ (mm)	$V_{peak}$ (kN)	$\Delta_{peak}$ (mm)	$v_u$ (MPa)	$v_u/\sqrt{f_c}$
S2.5-A-1	36.2	1.1	9.7	80.0	3.1	125.0	4.8	179.0	6.4	322.3	18.0	329.2	20.4	7.2	0.63
S2.5-A-2	30.1	0.9	8.1	80.0	2.7	125.0	3.0	175.0	4.5			308.0	17.6	6.8	0.59
S2.5-C-1	34.6	1.1	9.3	60.0	2.0	112.5	3.7	175.0	5.5	307.3	16.7	309.4	17.9	6.8	0.63
S2.5-C-2	32.0	1.1	8.6	55.0	1.6	205.0	5.8	250.0	7.1			307.1	20.6	6.7	0.62
S2-A-1	45.9	1.2	9.8	87.5	2.4	200.0	5.1	307.2	7.5	326.2	7.8	459.9	19.0	10.1	0.88
S2-A-2	51.5	1.8	11.0	90.0	3.0	162.5	4.9	262.5	7.2	340.9	9.0	420.9	25.2	9.3	0.80
S2-C-1	56.6	1.2	12.1	100.0	2.5	262.5	6.5	325.0	8.1	286.8	7.1	378.0	17.7	8.3	0.77
S2-C-2	61.4	1.5	13.2	100.0	2.5	145.0	3.6	300.0	6.7	245.2	5.3	405.1	18.1	8.9	0.82
S1.5-A-1	80.9	1.2	13.0	100.2	1.5	174.8	2.7	253.9	3.8			550.0	8.2	12.1	1.05
S1.5-A-2	75.3	1.3	12.1	75.3	1.3	100.2	1.8	204.1	3.4	485.0	10.4	500.0	11.8	11.0	0.95
S1.5-C-1	68.4	1.2	11.0	100.2	1.6	170.5	2.6	250.1	3.6	461.5	6.5	575.0	10.9	12.6	1.17
S1.5-C-2	68.4	1.2	11.0	100.2	1.6	150.0	2.4	174.8	2.8	365.2	5.6	575.0	13.5	12.6	1.17
S1-A-1	99.9	1.3	10.7	125.1	1.6	224.9	2.8	299.6	3.7	494.5	5.8	800.0	10.3	17.6	1.53
S1-A-2	99.9	1.6	10.7	99.9	1.6	199.7	2.9	224.9	3.2	494.3	6.4	750.0	9.0	16.5	1.43
S1-C-1	109.2	1.3	11.7	125.1	1.5	224.9	2.6	242.7	2.8	339.4	3.8	800.0	7.6	17.6	1.62
S1-C-2	93.3	0.8	10.0	99.9	0.9	175.5	2.0	324.8	3.6	513.0	5.7	750.0	9.5	16.5	1.52

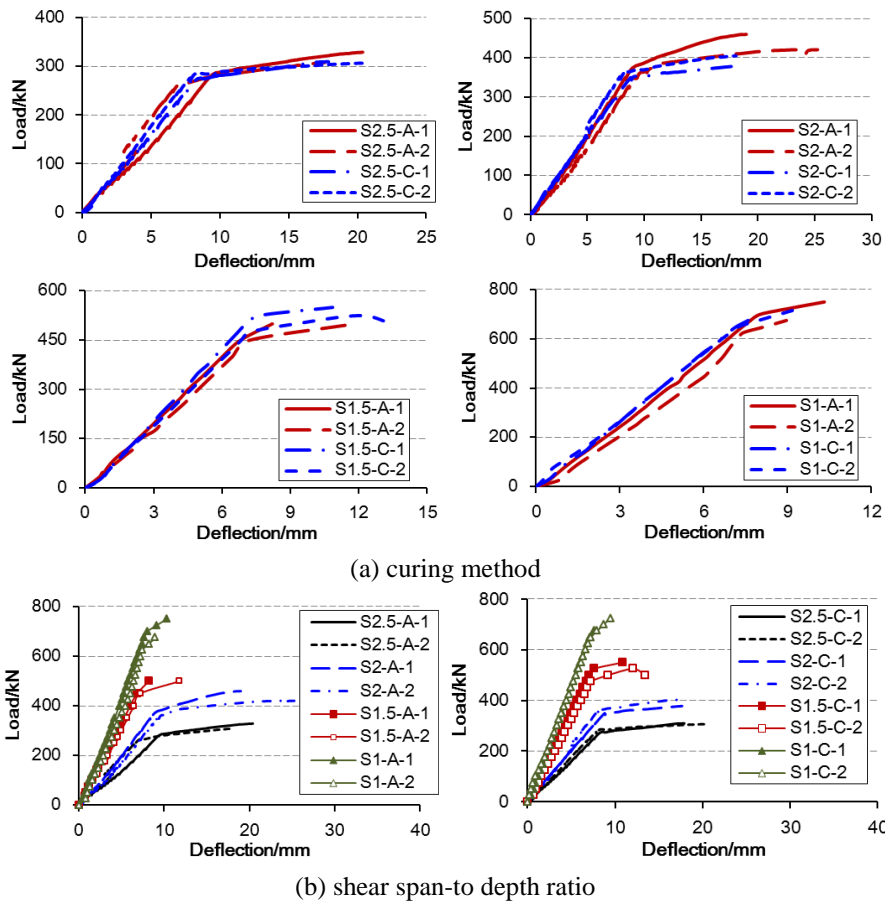


Fig. 8 Load versus mid-span deflection

approximate equivalent shear strengths were reached for same specimens no matter what curing method was used.

3.3 Structural behavior

**Load versus mid-span deflection** - The load versus mid-

span deflection responses for all specimens are presented in Fig. 8. It can be observed that all specimens exhibited similar behavior with a linear relationship between applied load and mid-span point deflection prior to the occurrence of visible flexural cracking. After flexural cracking, specimen stiffness was slightly reduced but still behaved

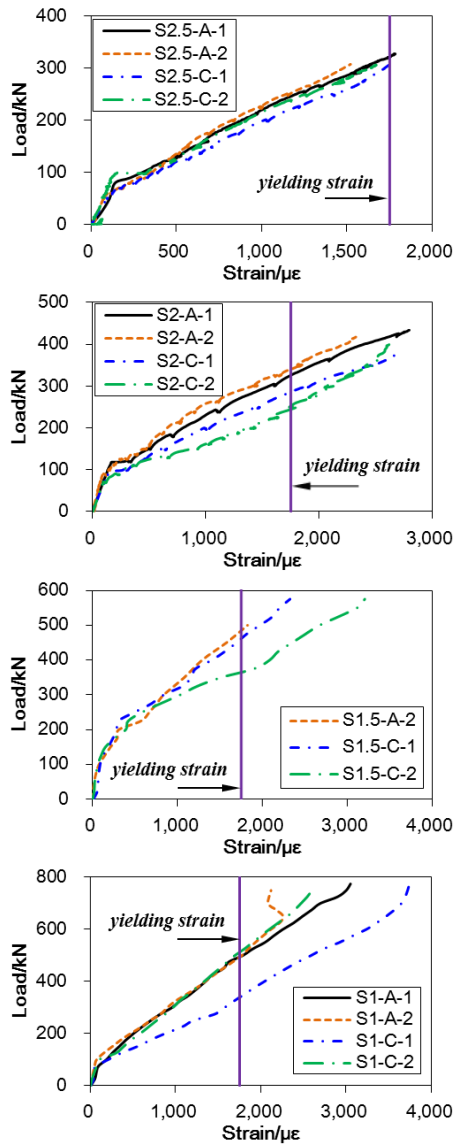


Fig. 9 Load versus shear span longitudinal reinforcement strain

approximately linearly. However, specimen stiffness was significantly reduced after the yielding of longitudinal reinforcement. For unloading process, specimen exhibited similar stiffness compared to the loading process but possessed a permanent deformation at last. Here, it is interesting to demonstrate that the curing method showed no significant influence on the load-deflection response of the test specimens in terms of specimen stiffness and ultimate capacity. The specimen stiffness increased as the shear span-to-height ratio decreased.

**Load versus longitudinal reinforcement strain** - The load-longitudinal reinforcement strain relationship was evaluated based on the strains measured by the strain gauges on the rebar surface. Fig. 9 shows the load-longitudinal reinforcement strain curves of all test specimens. Before cracking, strain in longitudinal reinforcement increased slowly with a linear behavior. After cracking, the strain increment in longitudinal reinforcement accelerated dramatically and still remained approximately

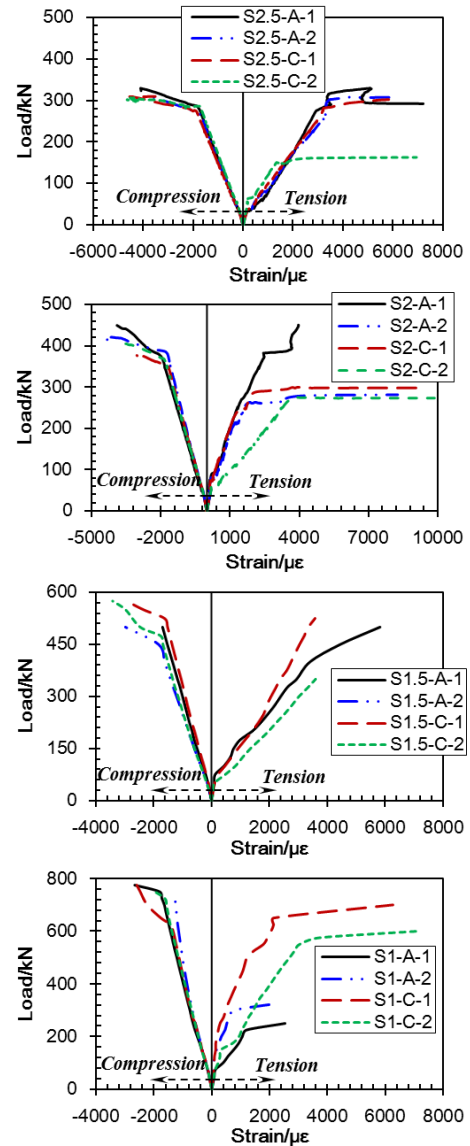


Fig. 10 Load versus top and bottom concrete surface strains of mid span section

linearly until the yielding state. The longitudinal reinforcement strain continued to increase after yielding corresponding to the rapid increasing of the specimen deflection. Lastly, the longitudinal reinforcement strain retained about 500 micro strains corresponding to the permanent deformation of the test specimen.

**Load versus top and bottom concrete surface strains of mid span section** - The load versus concrete surface strain of mid-span section for all test specimens are shown in Fig. 10. Positive strains represent tensile strains while negative strains represent compressive strains. Similar to load deflection response, the concrete compressive strains increased slowly before cracking, corresponding to the linear increment of the load deflection relationship. After cracking, the concrete compressive strains accelerated markedly until the yielding of longitudinal reinforcement, and then increased with a fastest increment until failure. For tension side, the tensile strain remained around zero before cracking and increased significantly after the appearance of

visible flexural cracks. The strain gauges on the tension side were finally ruptured due to the over-limit tensile stress and the large opening the cracks.

## 4. Discussions

### 4.1 Global behaviour

UHPFRC members exhibit a similar elastic behavior compared to normal strength concrete and high strength concrete members before cracking. However, completely different post-cracking behavior is found in UHPFRC members, which can be summarized as follow:

(1) Fibers bridging mechanism begin to work immediately as the appearance of cracks and restrain the propagation of cracks until fibers completely being pulled out from the matrix. Therefore, the structural performance is significantly improved with the presence of steel fibers.

(2) More short fine cracks develop beside the existing cracks thanks to the randomly dispersed fibers, resulting in re-distributing and homogenizing of the concrete stress beside cracks and allowing for the occurrence of more cracks with a small spacing.

(3) Obviously audible sizzling sound could be heard during the loading process, corresponding to the phenomenon of fibers continuously being pulled out from the matrix.

(4) At failure, fibers are pulled out from the matrix or fractured across the cracks, significantly increasing the ultimate strength and ductility.

### 4.2 Shear strength

In order to compare the ultimate shear strengths of reinforced concrete (RC) members, steel fiber reinforced concrete (SFRC) members and UHPFRC members in this study, nominal shear strength was utilized. The nominal shear strength is defined as ultimate load divided by web width and effective depth, of the cross section and can be calculated by

$$v_u = \frac{V_u}{bd} \quad (1)$$

where  $V_u$  is shear strength;  $b$  is web width;  $d$  is effective depth.

In the previous study, a shear database of RC members and SFRC members collected from numerous literatures was established (Qi 2013, 2018). In this study, the database was filtered with the principle of members containing no stirrups and the shear span-to-height ratio ranging from 1 to 4. In total, 1480 RC members and 500 SFRC members were contained to compare with the test UHPFRC members. For RC members, the effective depth, concrete strength and longitudinal reinforcement ratio of the filtered members were  $20 \text{ mm} \leq d \leq 3000 \text{ mm}$ ,  $6.1 \text{ MPa} \leq f_c \leq 127.5 \text{ MPa}$  and  $0.1\% \leq \rho_s \leq 9.28\%$  respectively. For SFRC members, the effective depth, concrete strength, longitudinal reinforcement ratio and the fiber volume fraction of the filtered members were  $80 \text{ mm} \leq d \leq 1440 \text{ mm}$ ,  $19.6 \text{ MPa} \leq f_c \leq 111.5 \text{ MPa}$ ,  $0.37\% \leq \rho_s \leq 6.5\%$  and  $0.22\% \leq \rho_f \leq 3\%$

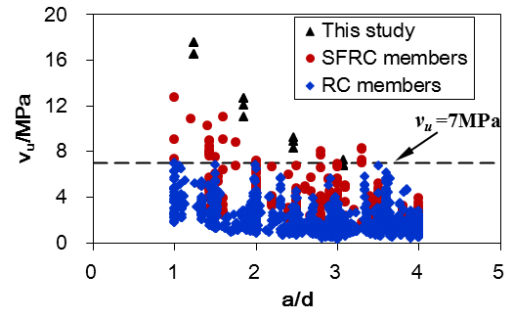


Fig. 11 Comparison of nominal shear strength

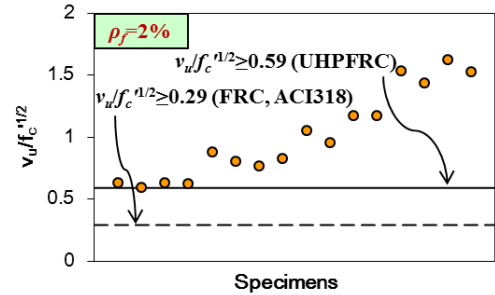


Fig. 12 Lower bound of normalized shear strength for UHPFRC specimen

respectively.

Fig. 11 presents the comparison result of the nominal shear strength between UHPFRC, SFRC and RC members. The nominal shear strengths of UHPFRC members in this study are generally larger than 7 MPa, whereas these values for conventional RC members are all below 7 MPa. The average values of nominal shear strength of the test specimens and RC members are about 11 MPa and 2 MPa. In case of SFRC members, more than 90% members have a nominal shear strength less than 7 MPa and the average nominal shear strength is about 3.5 MPa. Based on the above results, one can conclude that the nominal shear strength of UHPFRC members with 2% straight steel fibers is approximately 5.5 times as much as for conventional members and 3 times as much as for SFRC members.

### 4.3 Post-cracking capacity and deformability

For normal strength concrete members, brittle and sudden shear failure would occur after shear cracking, indicating that no sufficient shear strength reserve ability after shear cracking. However, the situation is different for UHPFRC members and considerable shear strength reserve ability could be obtained according to the test results (Qi *et al.* 2016). Therefore, four new indices were proposed to evaluate the post-cracking capacity of the test specimens, which were expressed in the form of dividing ultimate capacity by different cracking forces, including first cracking state, crack width of 0.05 mm, crack width of 0.10 mm and crack width of 0.15 mm. As shown in Table 6, the ultimate capacity could be as much as 8 times the cracking strength, 5 times the load at crack width of 0.05 mm, 3 times the load at crack width of 0.10 mm and 2 times the load at crack width of 0.15 mm. It can be seen that

Table 6 Post-cracking capacity and deformability analysis

Specimen ID	Post-cracking capacity				Ductility index				
	$V_u/V_{cr}$	$V_u/V_{0.05}$	$V_u/V_{0.10}$	$V_u/V_{0.15}$	$\Delta_{0.05}/\Delta_{cr}$	$\Delta_{0.10}/\Delta_{cr}$	$\Delta_{0.15}/\Delta_{cr}$	$\Delta_{peak}/\Delta_y$	$\Delta_{peak}/\Delta_{cr}$
S2.5-A-1	9.1	4.1	2.6	1.8	2.8	4.3	5.8	1.1	18.4
S2.5-A-2	10.2	3.9	2.5	1.8	2.9	3.4	5.0		19.5
S2.5-C-1	8.9	5.2	2.7	1.8	1.8	3.4	5.0	1.1	16.3
S2.5-C-2	9.6	5.6	1.5	1.2	1.5	5.5	6.7		19.4
S2-A-1	10.0	5.3	2.3	1.5	2.0	4.3	6.2	2.4	15.8
S2-A-2	8.2	4.7	2.6	1.6	1.7	2.8	4.1	7.6	14.3
S2-C-1	6.7	3.8	1.4	1.2	2.0	5.3	6.6	2.5	14.3
S2-C-2	6.6	4.1	2.8	1.4	1.6	2.3	4.4	3.4	11.9
S1.5-A-1	6.8	5.5	3.1	2.2	1.2	2.2	3.2		6.8
S1.5-A-2	6.6	6.6	5.0	2.4	1.0	1.3	2.6	1.1	8.9
S1.5-C-1	8.4	5.7	3.4	2.3	1.3	2.2	3.0	1.7	9.0
S1.5-C-2	8.4	5.7	3.8	3.3	1.4	2.0	2.3	2.4	11.2
S1-A-1	8.0	6.4	3.6	2.7	1.2	2.2	2.9	1.8	8.2
S1-A-2	7.5	7.5	3.8	3.3	1.0	1.8	2.0	1.4	5.5
S1-C-1	7.3	6.4	3.6	3.3	1.2	2.0	2.2	2.0	5.8
S1-C-2	8.0	7.5	4.3	2.3	1.2	2.4	4.5	1.7	11.8

UHPFRC members show superior load resistance after the appearance and propagation of cracks.

In general, the ductility of a concrete member can be characterized through ductility index, which can be expressed in the forms of deflection, curvature and rotational ductility index (Lee and Pan 2003, Pan *et al.* 2001, Qi *et al.* 2018b, Yoo and Yoon 2015). Deflection ductility index was chosen here for its convenient and simplicity. As shown in Table 6, excellent post-cracking deformability was obtained. Generally, the ductility index increases as the shear span-to-height ratio increases.

#### 4.4 Steel fibers as shear reinforcement

According to ACI 318-14 (2014), the steel fibers can be used as the shear reinforcement for SFRC members when the normalized shear strength is greater than  $0.29f_c^{1/2}$ . Parra-Montesinos (2006) pointed out that the shear strength of SFRC beam strength was larger than  $0.3f_c^{1/2}$  (MPa) when fiber content ( $\rho_f$ ) is equal to or greater than 0.75% based on the test results. Lim and Hong (2016) demonstrated that the rectangular beam contains UHPFRC with fiber volume fraction of 1.5% shear reinforcement need not be provided. In this study, the normalized shear strength of all test specimens with the steel fiber dosage of 2% were larger than  $0.59f_c^{1/2}$  as shown in Fig. 12. These results indicate that shear reinforcement need not be provided for UHPFRC decks with fiber volume fraction of 2%.

## 5. Comparison with current shear provisions

The current shear provisions, including French Code (AFGC-S etra), Mode Code 2010 (CEB-FIP 2012) and Chinese Code (CECS 38: 2004) were selected to predict the shear strength of the test specimens. The shear strength equations in different codes are explicitly expressed as follow.

In French Code, the summation of shear contributions from concrete, transverse reinforcement and fibers is used

$$V_u = V_{Rb} + V_a + V_f \quad (2)$$

$$V_{Rb} = \frac{1}{\gamma_E} \frac{0.21}{\gamma_b} k \sqrt{f_{cj}} b_0 d \quad (3)$$

$$V_a = \frac{A_{sw}}{s} df_{ywd} \cot \theta \quad (4)$$

$$V_f = \frac{S \sigma_p}{\gamma_{bf} \tan \beta_u} \quad (5)$$

$$\sigma_p = \frac{1}{K} \frac{1}{w_{lim}} \int_0^{w_{lim}} \sigma(w) dw \quad (6)$$

where  $V_{Rb}$  is the shear contribution of the concrete;  $V_a$  is the shear contribution of the stirrups;  $V_f$  is the shear contribution of the fibers;  $f_{cj}$  is compressive strength of UHPFRC;  $b_0$  is the width of the web;  $d$  is the effective depth;  $k$  is a factor that considers the effect of prestressing and is 1 for beams without prestressing;  $\gamma_E \gamma_b$  is the coefficient to characterize the uncertainty associated with UHPC;  $A_{sw}$  and  $s$  are the area and spacing of the stirrups, respectively;  $f_{ywd}$  is the yielding strength of the stirrups;  $\theta$  is the compressive stress field inclination;  $S$  is the resistance area of fibers, estimated with  $0.9b_0d$  for rectangular or Tee sections;  $\beta_u$  is the inclination of diagonal compression struts;  $\gamma_{bf}$  is the partial safety factor and equals to 1.3;  $\sigma_p$  is the residual tensile strength;  $K$  is the orientation coefficient;  $w_{lim}$  is the maximum crack width and is recommended to be 0.3 mm in the French Code;  $\sigma(w)$  is the stress at crack width  $w$ . In this study, the stress versus crack width relation is assumed to be linear and the residual tensile strength  $\sigma_p$  can be approximately estimated as the average of the stress level corresponding to zero crack width and a crack width limit of 0.3 mm.

Table 7 Shear strength prediction of current provisions

Specimen	Test		French Code: AFGC-Sétra					Mode Code 2010					Chinese Code: CECS 38: 2004					
	$V_u$ (kN)	$\sigma_p$ (MPa)	$V_{Rb}$ (kN)	$V_a$ (kN)	$V_f$ (kN)	$V_l$ (kN)	$V_u/V_1$	$V_{Rd,F}$ (kN)	$V_{Rd,s}$ (kN)	$V_2$ (kN)	$V_u/V_2$	$\beta_v$	$\lambda_f$	$V_c$ (kN)	$V_{fc}$ (kN)	$V_{sv}$ (kN)	$V_3$ (kN)	$V_u/V_3$
S2.5-A-1	329.2	6.1	123.0	0	249.8	372.8	0.88	307.1	0	307.1	1.07	0.7	1.3	225.5	430.7	0	430.7	0.76
S2.5-A-2	308	6.1	123.0	0	249.8	372.8	0.83	307.1	0	307.1	1.00	0.7	1.3	225.5	430.7	0	430.7	0.72
S2.5-C-1	309.4	6.0	115.7	0	245.7	361.4	0.86	292.9	0	292.9	1.06	0.7	1.3	212.2	405.2	0	405.2	0.76
S2.5-C-2	307.1	6.0	115.7	0	245.7	361.4	0.85	292.9	0	292.9	1.05	0.7	1.3	212.2	405.2	0	405.2	0.76
S2-A-1	459.9	6.1	123.0	0	249.8	372.8	1.23	307.1	0	307.1	1.50	0.7	1.3	225.5	430.7	0	430.7	1.07
S2-A-2	420.9	6.1	123.0	0	249.8	372.8	1.13	307.1	0	307.1	1.37	0.7	1.3	225.5	430.7	0	430.7	0.98
S2-C-1	378	6.0	115.7	0	245.7	361.4	1.05	292.9	0	292.9	1.29	0.7	1.3	212.2	405.2	0	405.2	0.93
S2-C-2	405.1	6.0	115.7	0	245.7	361.4	1.12	292.9	0	292.9	1.38	0.7	1.3	212.2	405.2	0	405.2	1.00
S1.5-A-1	550	6.1	123.0	0	249.8	372.8	1.48	307.1	0	307.1	1.79	0.7	1.3	225.5	430.7	0	430.7	1.28
S1.5-A-2	500	6.1	123.0	0	249.8	372.8	1.34	307.1	0	307.1	1.63	0.7	1.3	225.5	430.7	0	430.7	1.16
S1.5-C-1	575	6.0	115.7	0	245.7	361.4	1.59	292.9	0	292.9	1.96	0.7	1.3	212.2	405.2	0	405.2	1.42
S1.5-C-2	575	6.0	115.7	0	245.7	361.4	1.59	292.9	0	292.9	1.96	0.7	1.3	212.2	405.2	0	405.2	1.42
S1-A-1	800	6.1	123.0	0	249.8	372.8	2.15	307.1	0	307.1	2.61	0.7	1.3	225.5	430.7	0	430.7	1.86
S1-A-2	750	6.1	123.0	0	249.8	372.8	2.01	307.1	0	307.1	2.44	0.7	1.3	225.5	430.7	0	430.7	1.74
S1-C-1	800	6.0	115.7	0	245.7	361.4	2.21	292.9	0	292.9	2.73	0.7	1.3	212.2	405.2	0	405.2	1.97
S1-C-2	750	6.0	115.7	0	245.7	361.4	2.08	292.9	0	292.9	2.56	0.7	1.3	212.2	405.2	0	405.2	1.85
Average											1.40							1.23
SD											0.49							0.43

Note: SD=standard deviation.

The shear resistance for fiber reinforced concrete elements in Mode Code 2010 is given by

$$V_{Rd} = V_{Rd,F} + V_{Rd,s} \quad (7)$$

$$V_{Rd,F} = \left\{ \frac{0.18}{\gamma_c} k [100\rho_1 (1 + 7.5 \frac{f_{Fnk}}{f_{ck}}) f_{ck}]^{1/3} + 0.15\sigma_{cp} \right\} b_w d \quad (8)$$

$$V_{Rd,s} = \frac{A_{sw}}{s_w} z f_{ywd} \cot \theta \quad (9)$$

where  $\gamma_c$  is the partial safety factor;  $k$  is a factor that considers size effect,  $k = 1 + \sqrt{200/d} \leq 2.0$ ;  $\rho_1$  is the longitudinal reinforcement ratio;  $f_{Fnk}$  is the characterize value of the ultimate residual tensile strength;  $f_{ck}$  is the characterize value of the tensile strength for the concrete without fibers;  $f_{ck}$  is the characterize value of cylindrical compressive strength;  $\sigma_{cp}$  is the average stress acting on the concrete cross-section;  $b_w$  is the web width;  $d$  is the effective depth;  $A_{sw}$  is the area of stirrups;  $s_w$  is the spacing of stirrups;  $z$  is the effective shear depth;  $f_{ywd}$  is the yield strength of stirrups;  $\theta$  is the compressive stress field inclination.

Unlike calculating fibers shear contribution individually in the French Code, the Chinese Code is based on the shear design provisions for conventional reinforced concrete beams and multiplies an increase coefficient on concrete shear contribution to consider the effect of steel fibers

$$V_u = V_{fc} + V_{sv} \quad (10)$$

$$V_{fc} = V_c (1 + \beta_v \lambda_f) \quad (11)$$

$$V_c = 0.7 f_t b h_0 \quad (12)$$

$$V_{sv} = f_{yv} \frac{A_{sv}}{s} h_0 \quad (13)$$

where  $V_{fc}$  is the shear contribution of fiber reinforced concrete;  $V_{sv}$  is the shear contribution of stirrups;  $V_c$  is the shear contribution of concrete of conventional reinforced concrete beams;  $\beta_v$  is a factor that considers the effect of fiber's shape and is 0.7 for smooth straight fiber;  $\lambda_f$  is the characteristic value of steel fiber,  $\lambda_f = \rho_f l_f / d_f$ ;  $f_t$  is the tensile strength of concrete;  $b$  is the web width;  $h_0$  is the effective depth;  $f_{yv}$  is the yield strength of stirrups;  $A_{sv}$  is the area of stirrups;  $s$  is the spacing of stirrups.

The design safety factors  $\gamma_E$ ,  $\gamma_b$ ,  $\gamma_{bf}$  and  $\gamma_c$  were set to 1, and the compression struts angle  $\beta_u$  and compressive stress field inclination  $\theta$  were assumed to be 45°. The tensile strength of UHPFRC was taken as  $0.55f_c'1/2$  (Graybeal 2006). Table 7 shows the experimental shear strength as well as the predictions obtained by the current shear provisions. The average values of the ratios of the experimental results to French Code, Mode Code 2010 and Chinese Code predictions are 1.40, 1.71 and 1.23, with a standard deviation of 49%, 60% and 43%, respectively. All the three design codes gave a relative small shear strength prediction for specimens with small shear span-to-height ratio.

## 6. Conclusions

Sixteen rectangular specimens were tested to failure to investigate the structural performance of an innovative UHPFRC deck with coarse aggregate of composite bridge

under shear force. Based on the test observations and results, the conclusions are summarized as follows:

- Curing method, including steam curing and natural curing, did not have obvious effect on the nominal bending cracking strength and the ultimate strength of the test specimens, indicating that cast-in-place method could be used for UHPC structures construction.
- Shear reinforcement need not be provided for UHPFRC decks with a fiber volume fraction of 2%.
- UHPFRC decks show superior load resistance after the appearance of cracks and excellent post-cracking deformability. The nominal shear strength of UHPFRC members with 2% straight steel fibers is approximately 5.5 times as much as for conventional RC members and 3 times as much as for SFRC members.
- The average values of the ratios of the experimental results to French Code, Mode Code 2010 and Chinese Code predictions are 1.40, 1.71 and 1.23, with a standard deviation of 49%, 60% and 43%, respectively. All the three design codes are generally conservative in predicting the shear strength of the test specimens.

## Acknowledgments

This research was supported by the National Natural Science Foundation of China (Grant No. 51438003), the Fundamental Research Funds for the Central Universities (2242019K40073) and the Project of Research on Key Technology of Maintenance and Renovation of Nanjing Yangzi River Highway Bridge (201727002). Their support is greatly appreciated.

## References

- ACI (American Concrete Institute) (2014), Building Code Requirements for Structural Concrete (ACI 318-14) and Commentary, ACI 318R-14, Farmington Hills, MI.
- Akçaoğlu, T., Tokyay, M. and Çelik, T. (2004), "Effect of coarse aggregate size and matrix quality on ITZ and failure behavior of concrete under uniaxial compression", *Cement Concrete Compos.*, **26**(6), 633-638. [https://doi.org/10.1016/S0958-9465\(03\)00092-1](https://doi.org/10.1016/S0958-9465(03)00092-1).
- CEB-FIP (2012), Bulletin d'Information 65&66-Model Code MC2010 Final Draft, International Federation for Structural Concrete (fib), Lausanne, Switzerland.
- CECS 38: 2004 (2004), Technical Specification for Fiber Reinforced Concrete Structures, China Planning Press, Beijing.
- CECS13-2009 (2009), Standard Test Methods for Fiber Reinforced Concrete, China Planning Press, Beijing.
- French Association of Civil Engineering-French Authorities of Civil Engineering Structure Design, and Control (AFGC-Sétra) (2013), Ultra High Performance Fibre-Reinforced Concretes, Recommendations, Bagneux, France.
- GB/T 31387-2015 (2015), Reactive Powder Concrete, General Administration of Quality Supervision, Inspection and Quarantine of the People's Republic of China, Beijing.
- GB/T 50081-2002 (2002), Standard for Test Method of Mechanical Properties on Ordinary Concrete, Ministry of Construction of the People's Republic of China, Beijing.
- Ghasemi, S., Zohrevand, P., Mirmiran, A., Xiao, Y. and Mackie, K. (2016), "A super lightweight UHPC-HSS deck panel for movable bridges", *Eng. Struct.*, **113**, 186-193. <https://doi.org/10.1016/j.engstruct.2016.01.046>.
- Graybeal, B.A. (2006), "Material property characterization of ultra-high performance concrete (No. FHWA-HRT-06-103)", Federal Highway Administration, Office of Infrastructure Research and Development, United States.
- Harris, D.K. and Roberts-Wollmann, C.L. (2005), "Characterization of the punching shear capacity of thin ultra-high performance concrete slabs", Final Report, Virginia Transportation Research Council, Charlottesville, VA.
- Lachance, F., Charron, J.P. and Massicotte, B. (2016), "Development of precast bridge slabs in high-performance fiber-reinforced concrete and ultra-high-performance fiber-reinforced concrete", *ACI Struct. J.*, **113**(5), 929-939.
- Lee, T.K. and Pan, A.D.E. (2003), "Estimating the relationship between tension reinforcement and ductility of reinforced concrete beam sections", *Eng. Struct.*, **25**(8), 1057-1067. [https://doi.org/10.1016/S0141-0296\(03\)00048-8](https://doi.org/10.1016/S0141-0296(03)00048-8).
- Lim, W.Y. and Hong, S.G. (2016), "Shear tests for ultra-high performance fiber reinforced concrete (UHPFRC) beams with shear reinforcement", *Int. J. Concrete Struct. Mater.*, **10**(2), 177-188. <https://doi.org/10.1007/s40069-016-0145-8>.
- Liu, J., Han, F., Cui, G., Zhang, Q., Lv, J., Zhang, L. and Yang, Z. (2016), "Combined effect of coarse aggregate and fiber on tensile behavior of ultra-high performance concrete", *Constr. Build. Mater.*, **121**, 310-318. <https://doi.org/10.1016/j.conbuildmat.2016.05.039>.
- Ma, J., Orgass, M., Dehn, F., Schmidt, D. and Tue, N.V. (2004), "Comparative investigations on ultra-high performance concrete with and without coarse aggregates", *Proceedings of International Symposium on Ultra High Performance Concrete*, Germany.
- Mosaberpanah, M.A. and Eren, O. (2017), "Effect of quartz powder, quartz sand and water curing regimes on mechanical properties of UHPC using response surface modelling", *Adv. Concrete Constr.*, **5**(5), 481-492. <https://doi.org/10.12989/acc.2017.5.5.481>
- Naaman, A.E. and Chandrangsou, K. (2004), "Innovative bridge deck system using high-performance fiber-reinforced cement composites", *ACI Struct. J.*, **101**(1), 57-64.
- Naaman, A.E., Likhitrungsilp, V. and Parra-Montesinos, G. (2007), "Punching shear response of high-performance fiber-reinforced cementitious composite slabs", *ACI Struct. J.*, **104**(2), 170-179.
- Pan, H.J., Kwan, A.K.H. and Ho, J.C.M. (2001), "Post-peak behavior and flexural ductility of doubly reinforced normal-and high-strength concrete beams", *Struct. Eng. Mech.*, **12**(5), 459-474. <https://doi.org/10.12989/sem.2001.12.5.459>.
- Parra-Montesinos, G.J. (2006), "Shear strength of beams with deformed steel fibers", *Concrete Int.*, **28**(11), 57-66.
- Pourbaba, M., Joghataie, A. and Mirmiran, A. (2018), "Shear behavior of ultra-high performance concrete", *Constr. Build. Mater.*, **183**, 554-564. <https://doi.org/10.1016/j.conbuildmat.2018.06.117>.
- Pourbaba, M., Sadaghian, H. and Mirmiran, A. (2019), "A comparative study of flexural and shear behavior of ultra-high-performance fiber-reinforced concrete beams", *Adv. Struct. Eng.*, 1369433218823848. <https://doi.org/10.1177/1369433218823848>.
- Qi, J. (2013), "Theoretical and experimental study of shear strength for RC&PC&EPC bridge", Master's Thesis, Southeast University, Nanjing, China. (in Chinese)
- Qi, J. (2018), "Experimental and theoretical study on design method of UHPC beams based on multiscale analysis of interfacial bond behavior", Doctoral Thesis, Southeast University, Nanjing, China. (in Chinese)
- Qi, J., Hu, Y., Wang, J. and Li, W. (2018a), "Behavior and

- strength of headed stud shear connectors in ultra-high performance concrete of composite bridges”, *Front. Struct. Civil Eng.*, 1-12. <https://doi.org/10.1007/s11709-019-0542-6>.
- Qi, J., Ma, Z.J., Wang, J. and Liu, T. (2016), “Post-cracking shear strength and deformability of HSS-UHPFRC beams”, *Struct. Concrete*, **17**(6), 1033-1046. <https://doi.org/10.1002/suco.201500191>.
- Qi, J., Ma, Z.J. and Wang, J. (2017a), “Shear strength of UHPFRC beams: mesoscale fiber-matrix discrete model”, *J. Struct. Eng.*, **143**(4), 04016209. [https://doi.org/10.1061/\(ASCE\)ST.1943-541X.0001701](https://doi.org/10.1061/(ASCE)ST.1943-541X.0001701).
- Qi, J., Wang, J. and Ma, Z.J. (2018b), “Flexural response of high-strength steel-ultra-high-performance fiber reinforced concrete beams based on a mesoscale constitutive model: experiment and theory”, *Struct. Concrete*, **19**(3), 719-734. <https://doi.org/10.1002/suco.201700043>.
- Qi, J., Wang, J., Li, M. and Chen, L. (2017b), “Shear capacity of stud shear connectors with initial damage: Experiment, FEM model and theoretical formulation”, *Steel Compos. Struct.*, **25**(1), 79-92. <https://doi.org/10.12989/scs.2017.25.1.079>.
- Qi, J., Wu, Z., Ma, Z.J. and Wang, J. (2018c), “Pullout behavior of straight and hooked-end steel fibers in UHPC matrix with various embedded angles”, *Constr. Build. Mater.*, **191**, 764-774. <https://doi.org/10.1016/j.conbuildmat.2018.10.067>.
- Saleem, M.A., Mirmiran, A., Xia, J. and Mackie, K. (2011), “Ultra-high-performance concrete bridge deck reinforced with high-strength steel”, *ACI Struct. J.*, **108**(5), 601-609.
- Saleem, M.A., Mirmiran, A., Xia, J. and Mackie, K. (2014), “Experimental characterization of ultrahigh-performance concrete bridge deck system”, *J. Bridge Eng.*, **20**(9), 04014101. [https://doi.org/10.1061/\(ASCE\)BE.1943-5592.0000697](https://doi.org/10.1061/(ASCE)BE.1943-5592.0000697).
- Suwaed, A.S. and Karavasilis, T.L. (2018), “Removable shear connector for steel-concrete composite bridges”, *Steel Compos. Struct.*, **29**(1), 107-123. <https://doi.org/10.12989/scs.2018.29.1.107>.
- Tasdemir, C., Tasdemir, M.A., Lydon, F.D. and Barr, B.I. (1996), “Effects of silica fume and aggregate size on the brittleness of concrete”, *Cement Concrete Res.*, **26**(1), 63-68. [https://doi.org/10.1016/0008-8846\(95\)00180-8](https://doi.org/10.1016/0008-8846(95)00180-8).
- Toutlemonde, F., Resplendino, J., Sorelli, L., Bouteille, S. and Brisard, S. (2005), “Innovative design of ultra high-performance fiber reinforced concrete ribbed slab: experimental validation and preliminary detailed analyses”, *7th International Symposium on Utilization of High Strength/High Performance Concrete*, Washington DC, USA.
- Tran, N.T., Tran, T.K. and Kim, D.J. (2015), “High rate response of ultra-high-performance fiber-reinforced concretes under direct tension”, *Cement Concrete Res.*, **69**, 72-87. <https://doi.org/10.1016/j.cemconres.2014.12.008>.
- Walter, R., Olesen, J.F., Stang, H. and Vejrum, T. (2007), “Analysis of an orthotropic deck stiffened with a cement-based overlay”, *J. Bridge Eng.*, **12**(3), 350-363. [https://doi.org/10.1061/\(ASCE\)1084-0702\(2007\)12:3\(350\)](https://doi.org/10.1061/(ASCE)1084-0702(2007)12:3(350)).
- Wang, C., Yang, C., Liu, F., Wan, C. and Pu, X. (2012), “Preparation of ultra-high performance concrete with common technology and materials”, *Cement Concrete Compos.*, **34**(4), 538-544. <https://doi.org/10.1016/j.cemconcomp.2011.11.005>.
- Wang, J., Qi, J., Tong, T., Xu, Q. and Xiu, H. (2019), “Static behavior of large stud shear connectors in steel-UHPC composite structures”, *Eng. Struct.*, **178**, 534-542. <https://doi.org/10.1016/j.engstruct.2018.07.058>.
- Yoo, D.Y. and Yoon, Y.S. (2015), “Structural performance of ultra-high-performance concrete beams with different steel fibers”, *Eng. Struct.*, **102**, 409-423. <https://doi.org/10.1016/j.engstruct.2015.08.029>.